ACS APPLIED MATERIALS & INTERFACES

Letter

www.acsami.org

Improving Efficiency by Hybrid TiO_2 Nanorods with 1,10-Phenanthroline as A Cathode Buffer Layer for Inverted Organic Solar Cells

Chunming Sun,[†,‡] Yulei Wu,[†] Wenjun Zhang,[†] Nianquan Jiang,[‡] Tonggang Jiu,*[,†] and Junfeng Fang*[,†]

[†]Ningbo Institute of Materials Technology and Engineering, Chinese Academy of Sciences, Ningbo, 315201, China

[‡]College of Physics & Electronic Information Engineering, Wenzhou University, Wenzhou 325035, China

Supporting Information

ABSTRACT: We reported a significant improvement in the efficiency of organic solar cells by introducing hybrid TiO_2:1,10-phenanthroline as a cathode buffer layer. The devices based on polymer thieno[3,4-b]thiophene/benzodithiophene:[6,6]-phenyl C_{71}-butyric acid methyl ester (PTB7:PC_{71}BM) with hybrid buffer layer exhibited an average power conversion efficiency (PCE) as high as 8.02%, accounting for 20.8% enhancement compared with the TiO_2 based devices. The cathode modification function of this hybrid material could also be extended to the poly(3-hexylthiophene):[6,6]-phenyl-C_{61}-butyric acid methyl ester (P3HT:PC_{61}BM) system. We anticipate that this study will stimulate further research on hybrid materials to achieve more efficient charge collection and device performance.

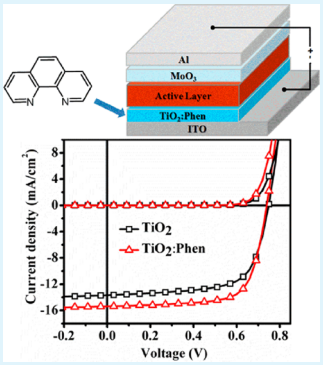

KEYWORDS: *hybrid buffer layer, inverted OSC, TiO_2, 1,10-phenanthroline*

1. INTRODUCTION

Organic solar cells (OSCs) based on bulk-heterojunctions (BHJ) structure have attracted great interest since 1995,[1] because of their advantages of low cost, light weight, and flexibility. During the past decade, the power conversion efficiency (PCE) of OSCs was improved significantly and has exceeded 9% in the scientific literature.[2] For traditional BHJ OSCs, the active layer containing an interpenetrating network of organic donor and fullerene was sandwiched between the transparent indium tin-oxide (ITO) and Al electrode.[3,4] To improve the charge carrier transport and collection ability, researchers used hole-conducting poly(3,4-ethylenedioxylene-thiophene):poly (styrene sulfonic acid) (PEDOT:PSS) and the low-work-function (WF) metal (Ca, Ba etc.) as the buffer layer.[5,6] However, both of them are potentially detrimental to the device stability because of their corrosive or oxidizing nature, which can cause interface instability and lead to device degradation and failure.[7,8] With respect to these issues, inverted device structure was invented as an alternative and has drawn considerable attention. In the inverted architecture, the charge carrier collection is opposite to that in the conventional architecture. This offers us the opportunity to use the high WF and less air-sensitive electrodes (Au, Cu, etc.) as the top electrode for hole collection.[9,10] The electron extraction buffer layer on transparent ITO electrode became the key issue for the high-performance OSCs. Many kinds of organic or inorganic buffer layer, such as PFN,[2,11] Cs_2CO_3,[12,13] ZnO,[14,15] CdS,[16] and TiO_x,[9,17−20] were developed and showed impressive photovoltaic performance.

Titanium dioxide (TiO_2) as a well-known n-type semiconductor has good transparency, high electron mobility, environmental friendliness, and high stability.[21] It has been widely studied because of its potential applications in photocatalysts,[22] dye-sensitized solar cells (DSSC),[23] and as the electron acceptor in hybrid OSCs.[24−26] From the electronic structure (energy level), TiO_2 is not only a suitable cathode interfacial layer for the electron-collecting but also a good hole-blocking layer because of its low-lying valence band. Apart from the electron extraction function, TiO_2 could also act as the optical spacer to improve light absorption in the devices.[20] Promising efficiencies with TiO_2 as the cathode buffer layer were reported.[20,27,28] To further improve the performance, the modification of adhesion and compatibility between the organic active layer and inorganic oxide are also important.[16,28,29] Self-assembled monolayer (SAM) or a cross-linkable fullerene layer on TiO_2 was reported as a successful method to improve the device performance.[30,31] But the drawbacks for SAM were probable desorption during wet processing and highly dependent on processing conditions.[32] The high selectivity cross-linkable groups also caused the complicated synthesis procedure.

In this work, we introduced an anatase titania nanorod (NR)/1,10-phenanthroline (Phen) hybrid cathode buffer layer, which was achieved simply by mixing Phen into the chloroform

Received: October 8, 2013
Accepted: December 27, 2013
Published: December 27, 2013

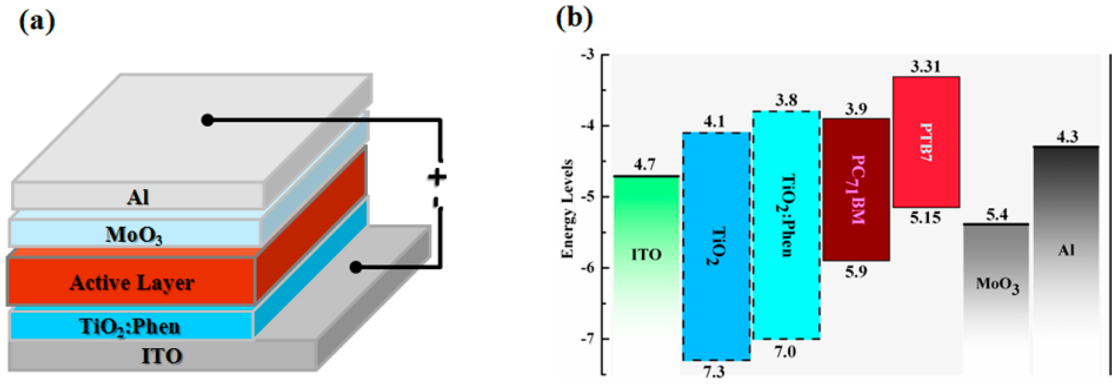

Figure 1. (a) Device structure of the inverted OSCs. (b) Corresponding energy levels diagram of the components involved in the inverted device.

solution of titania NRs, to improve the device performance. The increased delocalization of carriers in TiO_2 NRs is beneficial to the free movements of electron throughout the length of the crystal.[33,34] This is expected to improve the charge transport and collection ability in OSCs as well as reduce the electrons and holes recombination probability. Phen is a cost-effective material and commercial available for a long time as a chelating agent in the coordination chemistry. It was reported that Phen could enhance the electron transport of the organic metal complexes and also could block the holes and reduce the recombination[35−38] Inverted device with as-synthesized TiO_2 NRs showed a PCE of 6.64 ± 0.19% for polymer thieno[3,4-b]thiophene/benzodithiophene:[6,6]-phenyl C_{71}-butyric acid methyl ester (PTB7:$PC_{71}BM$), which confirmed the good cathode buffer function of TiO_2 NRs. After hybrid with Phen, inverted OSCs based on this blending buffer layer showed impressive improvement and exhibited a significant PCE up to 8.02 ± 0.09% under 100 mW/cm^2 AM 1.5G illumination. Over 20% enhancement was observed compared with the device with as-synthesized titania NRs (PCE = 6.64 ± 0.19%) as buffer layer under the same condition. We found that the interfacial modification of this hybrid material could also be extended to well-known poly(3-hexylthiophene):[6,6]-phenyl-C_{61}-butyric acid methyl ester (P3HT:$PC_{61}BM$) system (PCE of 4.02% achieved). The interaction between TiO_2 NRs and Phen, the corresponding morphology and electronic structure were further investigated and discussed.

2. RESULTS AND DISCUSSION

Figure 1a and 1b exhibit the inverted device structure and the energy levels diagram of the component materials, respectively. The valence band (VB) of TiO_2 was determined by ultraviolet photoelectron spectroscopy (UPS, see Figure S1 in the Supporting Information), and the band gap (E_g) was calculated from the UV absorption edge (see Figure S2 in the Supporting Information). The VB and the conduction band (CB) of the TiO_2 were 7.3 and 4.1 eV, respectively. About 0.3 eV shifting of VB and CB were observed for TiO_2:Phen film because of the Phen incorporation. The VB (7.0 eV) of hybrid TiO_2 is still quite low-lying relative to highest occupied molecular orbital (HOMO) of $PC_{71}BM$ (5.9 eV),[17] which indicated the still excellent hole blocking function. Because the CBs of both TiO_2 and TiO_2:Phen are close to the lowest unoccupied molecular orbital (LUMO) of $PC_{71}BM$, the facilitated electron transport from $PC_{71}BM$ to the ITO through both buffer layers is expected.[39]

The current density versus voltage (J−V) characteristics of the inverted devices based on PTB7:$PC_{71}BM$ under standard 1 sun (100 mW/cm^2) AM 1.5 simulated solar irradiation and in the dark condition are shown in Figure 2a. Table 1 summarized

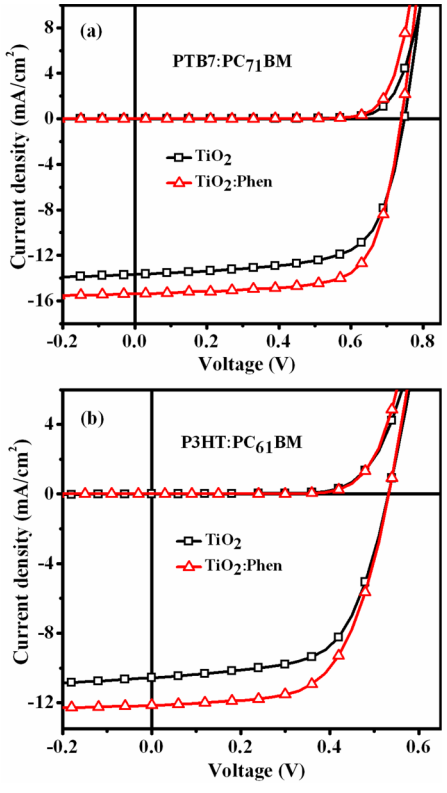

Figure 2. J−V curve of inverted devices (a) PTB7:$PC_{71}BM$ and (b) P3HT:$PC_{61}BM$ under 100 mW/cm^2 AM 1.5G illumination and in the dark.

the specific device parameters. Devices with as-synthesized TiO_2 NRs as the buffer layer showed a high PCE of 6.92%, with an open circuit voltage (V_{oc}) of 0.749 V and a short current density (J_{sc}) of 13.66 mA/cm^2. The fill factor (FF) reached 67.6% and the average PCE was 6.64%. When hybrid with Phen at an optimized weight ratio of 3:7, the devices showed an impressive improvements and the PCE was as high as 8.12% (see Table S1 in the Supporting Information). The average PCE was 8.02%, which was enhanced 20.8% compared with the TiO_2 based devices (6.64%). More importantly, the devices with TiO_2:Phen as the buffer layer had better reproducibility

dx.doi.org/10.1021/am404423k | ACS Appl. Mater. Interfaces 2014, 6, 739−744

Table 1. Specific Device Parameters with TiO_2 and TiO_2:Phen as the Buffer Layer Measured under 100 mW/cm^2 AM 1.5G Illumination (ITO/buffer layer/active layer/MoO_3/Al)

materials	active layer	V_{oc} [V]	J_{sc} (mA/cm^2)	FF (%)	η (%) best (average)	R_s (Ω cm^2)	R_{sh} Ω cm^2
TiO_2	PTB7:$PC_{71}BM$	0.749	13.66	67.6	6.92 (6.64 ± 0.19)	6.24	776
TiO_2:Phen		0.740	15.37	71.4	8.12 (8.02 ± 0.09)	4.88	1150
TiO_2	P3HT:$PC_{61}BM$	0.532	10.55	62.5	3.51 (3.11 ± 0.33)	9.04	566
TiO_2:Phen		0.533	12.13	62.2	4.02 (3.99 ± 0.05)	8.12	1010

[a]Average of eight devices. The device parameter distribution maps are presented in Figure S5 in the Supporting Information.

(smaller deviation). The series resistance (R_s) was decreased to 4.88 Ω cm^2 from 6.24 Ω cm^2 and the shunt resistance (R_{sh}) was increased to 1150 from 776 Ω cm^2. It indicated better interface properties in the devices, which will lead to more efficient electron collection and less charge carrier recombination. This was consistent with the improved J_{sc} and *FF* as presented in the Table 1. The result of the incident photon to current conversion efficiency (IPCE) measurements (see Figure S3 in the Supporting Information) with hybrid TiO_2:Phen was much higher at almost overall wavelength range compared with that of as-synthesized TiO_2 based devices. It further confirmed that the hybrid of inorganic TiO_2 NRs and organic Phen was an efficient method to improve the electron extraction for the inverted OSCs. The cathode modifying function of hybrid TiO_2:Phen for the different active materials was also investigated (Figure 2b). In addition to PTB7:$PC_{71}BM$ active layer, P3HT:$PC_{61}BM$, a well-known and widely studied system for OSCs, has been tested as the bulk hetero-junction layer. Compared with the as-synthesized TiO_2 (PCE = 3.11 ± 0.33%), the PCEs of TiO_2:Phen devices showed an improvement of 28% so that they reached to 3.99 ± 0.05%. Evidently, the interface modification of hybrid buffer materials does work for different active layers.

The crystalline phase of as-synthesized TiO_2, TiO_2:Phen, and Phen samples were studied by the X-ray powder diffraction (XRD) and the results were shown in Figure 3a. The XRD pattern for TiO_2 confirmed the existence of anatase TiO_2 nanocrystalline, which agreed well with the previous reported results.[34] All the peaks were ascribed to the anatase crystal structure without obvious secondary reaction crystalline phase. The XRD profile of the Phen sample belong to the monoclinic space group C2 recognized in the literature.[40,41] The XRD spectrum of TiO_2:Phen showed that the TiO_2:Phen matrix was a mixture of anatase TiO_2 nanocrystalline and Phen crystal. To further understand whether there was interaction between the interface of TiO_2 and Phen, we carried out X-ray photoelectron spectroscopy (XPS) characterization. Figure 3b shows titanium 2p core-level spectra (Figure 4b). The as-synthesized TiO_2 sample surface exhibited a Ti $2p_{3/2}$ peak centered at 458.8 eV and a Ti $2p_{1/2}$ peak centered at 464.5 eV, which are ascribed to Ti^{4+} bond to oxygen. However, hybrid sample (TiO_2:Phen) showed the peaks at 458.3 and 464.0 eV, respectively. The slight shifting of the Ti 2p peak to the lower binding energy implied the electronic structure change of TiO_2. It should be associated with the coordination bond formation between TiO_2 and Phen.[42] Furthermore, from the N 1s spectrum (see Figure S4 in the Supporting Information), the trace of nitrogen was not obvious in as-synthesized TiO_2 sample which was similar to the previous reported results,[43] but it appeared clearly in the hybrid TiO_2:Phen sample.[43] The N 1s binding energy of 399.9 eV in TiO_2:Phen may be assigned as a combine result of Ti−N and N−C which was located between TiN (Ti−N: 396.8 eV) and Phen (N−C: 401.3 eV).[44−46] The result was confirmed to be ascribed to the coordination bond formation in Phen based metal complexes.[30,44] The chemical interaction between TiO_2 and Phen could result in the formation of metal-ligand electron delocalization, which would facilitate electron transfer from Phen phase to TiO_2 NRs. Therefore, electron transport and collection in the OSCs will be more efficient.[40]

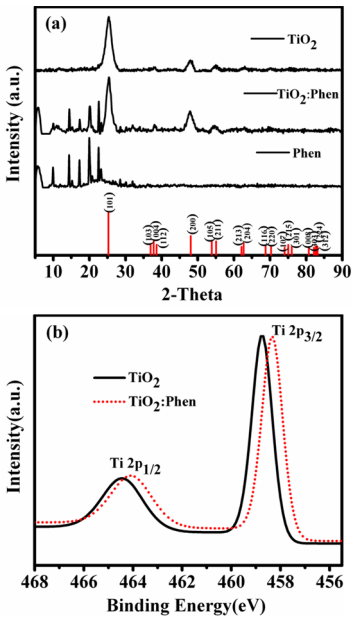

Figure 3. (a) X-ray diffraction patterns for as-synthesized TiO_2, TiO_2:Phen, and Phen after annealing at 150 °C for 15 min. (b) Titanium 2p core-level spectra of XPS analysis for the as-synthesized TiO_2 and TiO_2:Phen films surfaces.

The SEM images of as-synthesized TiO_2 and TiO_2:Phen films are shown in Figure 4a and 4b, respectively. The two images indicated that TiO_2 NRs were homogeneously and irregularly distributed in the films and several nanorods were bunched together. It was noted that TiO_2:Phen image was quite different from the as-synthesized TiO_2 one. Many darker domains, which were the Phen-rich parts, appeared. The TiO_2 nanoparticles were no longer separated individually. Instead, some nanoparticles gathered to form larger agglomerations. Furthermore, it can be observed that the particles or the agglomerations were permeated by a soft material of Phen and the gap size between the TiO_2 NRs was significantly decreased. This change, on the one hand, suggested that the organic Phen modification would significantly vary the morphology of the self-organized TiO_2 film during spin coating, which would lead to better accommodating ability between buffer material and active layer;[28] on the other hand, it could restrain the direct contact of the active layer with ITO electrode. Phen has good electronic property and is widely used as the ligand to synthesize organic electronic metal complexes.[37] As a result, the

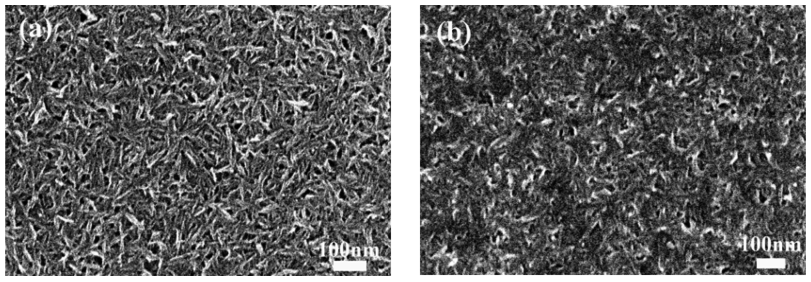

Figure 4. SEM images of the buffer layers annealed at 150°C for 15 min.: (a) as-synthesized TiO_2, (b) TiO_2:Phen.

introducing of the Phen will not only lead to expected morphology improvements but also guarantee the good electronic property for the electron to go through the interface smoothly. The improved contact area could benefit for the decrease of series resistance. The decreased risk of direct contact between active layer and ITO could also increase shunt resistance. These were well consistent with the device parameters summarized in Table 1.

Figure 5a and 5b show the atomic force microscopy (AFM) by tapping mode of as-synthesized TiO_2 and TiO_2:Phen on ITO substrate, respectively. In the case of TiO_2 NRs, the image showed an average roughness of 4.17 nm; on the other hand, the average roughness of the TiO_2:Phen top surface becomes 5.01 nm. The increased average roughness can provide a larger interfacial contact area between the active layer and buffer layer.[47,48] The electron collection from the $PC_{71}BM$ to the electrode through the hybrid TiO_2:Phen could be improved due to the larger contact area.[28,48] This will directly lead to the increase of the device current. Water contact angle measurement was further performed for as-synthesized TiO_2 film and hybrid TiO_2:Phen film in Figure S6a, b in the Supporting Information. The as-synthesized TiO_2 film exhibited a contact angle of 89.72°, which can be attributed to the adsorption of pyridine on TiO_2 nanorods.[28] Moreover, the water contact angle of the hybrid TiO_2:Phen film was further increased to 92.43° from 89.72° of the as-synthesized TiO_2 film. The increased hydrophobicity can be attributed to two reasons:[28] (1) the rougher surface features of TiO_2:Phen film (root mean square roughness = 6.39 nm) compared with the as-synthesized TiO_2 nanorods (root mean square roughness = 5.15 nm), and (2) the intrinsic hydrophobicity of the Phen mixed with TiO_2. Because of the hydrophobic solvent (chlorobenzene) used in the preparation of the active layer, the enhanced hydrophobicity of the buffer layer can help the flow and the spread of the active layer solution deposition on the buffer layer.[49] Consequently, it suggested that the Phen modification can facilitate the accommodating of the active layer in the three dimensional nanostructure. The improved interface properties should reduce the recombination of charge carriers at the interface and improve the device performance.[50,51]

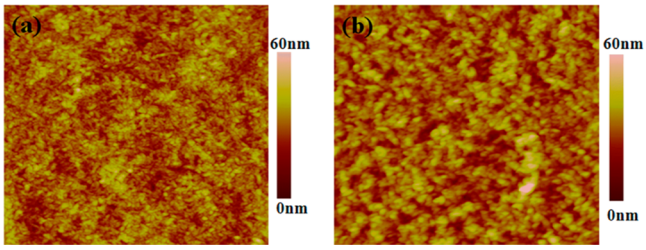

Figure 5. AFM images (2.0 × 2.0 μm) of the buffer layers: (a) as-synthesized TiO_2, (b) TiO_2:Phen.

3. CONCLUSION

In summary, we have fabricated inverted OSCs by using TiO_2 NRs and TiO_2:Phen hybrid materials as the cathode buffer layer. The hybrid film was prepared by simply mixing cost-effective Phen into the chloroform solution of TiO_2 NRs and then spin-coated to the ITO glass. The performance of the devices with the hybrid buffer layer TiO_2:Phen showed significant improvements compared with as-synthesized TiO_2. An average PCE of 8.02% was achieved, which was enhanced 20.8% compared with the as-synthesized TiO_2 based devices (6.64%). The significant improvements were also applied to the different photoactive system (PTB7:$PC_{71}BM$ and P3HT:$PC_{61}BM$). The incorporation of Phen will improve surface property of the hybrid film such as better contact, increased surface contact area and compatibility with the solvent of the active solution. We anticipate that this study will stimulate further research on hybrid materials to achieve more efficient charge collection and devices performance.

4. EXPERIMENTAL SECTION

Reagent and Materials. Indium tin oxide (ITO) coated glass substrates were obtained from CSG HOLDING CO. Electron donor material PTB7 was purchased from 1-material Chemscitech and electron acceptor $PC_{71}BM$ was purchased from American Dye Source, Inc. Chlorobenzene and 1,8-diiodoctane was provided by Sigma-Aldrich. In addition, the Titanium tetraisopropoxide (TTIP) was purchased from J&K Scientific Ltd. 1,10-Phenanthroline was purchased from Aladdin Chemical reagent Co. Ltd. (Shanghai, China). Methanol and chloroform were purchased from Sinopharm Chemical Reagent Co. All the chemicals were used as received without further purification.

Preparation of TiO_2 NRs and Ligand Exchange. Anatase TiO_2 NRs with a high aspect ratio were synthesized according to a reported method elsewhere.[34] The as-synthesized TiO_2 NRs are usually capped with an insulating surfactant of oleic acid (OA), comprised of a long alkyl chain, which acts as a potential barrier for the charge transfer. Therefore, ligand exchange treatment of TiO_2 replaces the original OA surfactant by pyridine, which was described according to a reported method.[24] The as-synthesized TiO_2 NRs were precipitated by methanol 3 times. The precipitant was then re-dispersed in pyridine (5ml, AR), and aided of an ultrasonic homogenizer. The TiO_2 nanocrystals/pyridine solution was then allowed to keep at 78°C for 4h till the solution turned clear. Finally, we used an excess of hexane to precipitate the pyridine-coated TiO_2 NRs at room temperature and to wash out the

dx.doi.org/10.1021/am404423k | ACS Appl. Mater. Interfaces 2014, 6, 739−744

nonadsorbed surface modifiers and isolated the resulting precipitates by centrifugation. These TiO_2 NRs modified with pyridine were then redispersed in chloroform. A solution of TiO_2:Phen was obtained by blending Phen at different weight ratios in chloroform solution.

Device Fabrication. BHJ PV devices were fabricated by the following procedure. The patterned ITO substrate was cleaned by ultrasonic treatment in detergent, deionized water, acetone, and isopropyl alcohol sequentially. The prepared solution of TiO_2:Phen was deposited on the ITO-coated glass substrate with 1500 rpm for 60s. The TiO_2:Phen films were annealed at 150°C for 15 min in the air. The thickness of TiO_2:Phen film is 10 nm. The polymer blend of P3HT:PC_{61}BM at a 20:20 weight ratio was spin-casted at 800 rpm for 40s on top of a layer of TiO_2:Phen buffer layer and followed by solvent annealing for 2 h. The polymer blend of PTB7:PC_{71}BM at a 1:1.5 weight ratio was spin-cast from mixed solvent of chlorobenzene/1,8-diiodoctane (97:3 vol %). Finally, the devices were pumped down to a ca. 1×10^{-6} mbar pressure, and a ca. 10 nm MoO_3 and a ca. 100 nm Al film was deposited on top of the photoactive layer through a shadow mask to obtain the active area size of 2×2 mm^2.

Characterization and Measurement. The light source was calibrated by using silicon reference cells with an AM 1.5 Global solar simulator with an intensity of 100 mW/cm^2. The *J*−*V* characteristics of the solar cells were measured by a Keithley 2400 source meter under exposure to AM 1.5 Global solar simulator with an intensity of 100 mW/cm^2. The EQE measurements were measured with The Newport IQE-200 Measurement System, which was equipped with a Xe lamp, a monochromator, a current−voltage preamplifier, and a lock-in amplifier. For XRD analysis, Bruker D8 advance X-ray diffractometer with Cu Kα radiation was used. The absorption spectra were measured by PerkinElmer Lambda 950 UV−vis−NIR spectrophotometer over the wavelength range between 300 and 800 nm. The surface morphologies of the specimens were obtained using SEM (S-4800) and atomic force microscope (AFM). AFM was operated in tapping mode by using a Veeco dimension V atomic microscope at room temperature. Water contact angle measurements were performed using Contact Angle System OCA-20. X-ray photoelectron spectroscopy (XPS) and ultraviolet photoelectron spectroscopy (UPS) were studied using a Kratos AXIS UTRADLD UPS/XPS system (Kratos analytical, Manchester, UK). XPS studies were performed on using a monochromated AlKα (1,486.6 eV) X-ray source. All recorded peaks were calibrated for electrostatic effects by setting the C−C component of the C1s Peak to 284.8 eV. UPS were using the He (I) (21.2 eV) line in order to shift the spectra from the spectrometer threshold. The spectra were calibrated vs the Fermi edge of polycrystalline Au.

■ ASSOCIATED CONTENT

Supporting Information

UPS spectra and UV−vis absorption spectra for TiO_2 and TiO_2:Phen film. EQE spectra of the inverted PTB7:PC_{71}BM and P3HT:PC_{61}BM devices with TiO_2, and TiO_2:Phen. XPS spectrum of nitrogen 1s core-level spectra. The device parameter distribution map using TiO_2, TiO_2:Phen as buffer layer in PTB7:PCB_{71}M system. This material is available free of charge via the Internet at http://pubs.acs.org.

■ AUTHOR INFORMATION

Corresponding Authors

*E-mail: jiutonggang@nimte.ac.cn.
*E-mail: fangjf@nimte.ac.cn.

Notes

The authors declare no competing financial interest.

■ ACKNOWLEDGMENTS

This work was supported by the National Natural Science Foundation of China (51273208 and 51202264) and the Hundred Talent Program of the Chinese Academy of Sciences; the Starting Research Fund of Team Talent (Y10801A01) at NIMTE; the Ningbo Natural Science Foundation of China (2012A610114).

■ REFERENCES

(1) Yu, G.; Gao, J.; Hummelen, J. C.; Wudl, F.; Heeger, A. J. *Science* **1995**, *270*, 1789−1791.
(2) He, Z.; Zhong, C.; Su, S.; Xu, M.; Wu, H.; Cao, Y. *Nat. Photon.* **2012**, *6*, 593−597.
(3) Li, G.; Shrotriya, V.; Huang, J.; Yao, Y.; Moriarty, T.; Emery, K.; Yang, Y. *Nat. Mater.* **2005**, *4*, 864−868.
(4) Kim, Y.; Cook, S.; Tuladhar, S. M.; Choulis, S. A.; Nelson, J.; Durrant, J. R.; Bradley, D. D.; Giles, M.; McCulloch, I.; Ha, C.-S. *Nat. Mater.* **2006**, *5*, 197−203.
(5) Eo, Y. S.; Rhee, H. W.; Chin, B. D.; Yu, J.-W. *Synth. Met.* **2009**, *159*, 1910−1913.
(6) Reese, M. O.; White, M. S.; Rumbles, G.; Ginley, D. S.; Shaheen, S. E. *Appl. Phys. Lett.* **2008**, *92*, 053307.
(7) De Jong, M.; Van Ijzendoorn, L.; De Voigt, M. *Appl. Phys. Lett.* **2000**, *77*, 2255−2257.
(8) Kawano, K.; Pacios, R.; Poplavskyy, D.; Nelson, J.; Bradley, D. D.; Durrant, J. R. *Sol. Energy Mater. Sol. Cells.* **2006**, *90*, 3520−3530.
(9) Waldauf, C.; Morana, M.; Denk, P.; Schilinsky, P.; Coakley, K.; Choulis, S.; Brabec, C. *Appl. Phys. Lett.* **2006**, *89*, 233517−233517-3.
(10) White, M.; Olson, D.; Shaheen, S.; Kopidakis, N.; Ginley, D. S. *Appl. Phys. Lett.* **2006**, *89*, 143517−143517-3.
(11) Yang, T.; Wang, M.; Duan, C.; Hu, X.; Huang, L.; Peng, J.; Huang, F.; Gong, X. *Energy Environ. Sci.* **2012**, *5*, 8208−8214.
(12) Liao, H.-H.; Chen, L.-M.; Xu, Z.; Li, G.; Yang, Y. *Appl. Phys. Lett.* **2008**, *92*, 173303.
(13) Xu, Z.; Chen, L. M.; Yang, G.; Huang, C. H.; Hou, J.; Wu, Y.; Li, G.; Hsu, C. S.; Yang, Y. *Adv.Funct. Mater.* **2009**, *19*, 1227−1234.
(14) Sun, Y.; Seo, J. H.; Takacs, C. J.; Seifter, J.; Heeger, A. J. *Adv.Mater.* **2011**, *23*, 1679−1683.
(15) Liang, Z.; Zhang, Q.; Wiranwetchayan, O.; Xi, J.; Yang, Z.; Park, K.; Li, C.; Cao, G. *Adv. Funct. Mater.* **2012**, *22*, 2194−2201.
(16) Wu, Y.; Zhang, W.; Li, X.; Min, C.; Jiu, T.; Zhu, Y.; Dai, N.; Fang, J. *Appl. Mater. Interfaces* **2013**, *5*, 10428−10432.
(17) Tan, Z. a.; Zhang, W.; Zhang, Z.; Qian, D.; Huang, Y.; Hou, J.; Li, Y. *Adv.Mater.* **2012**, *24*, 1476−1481.
(18) Savva, A.; Petraki, F.; Elefteriou, P.; Sygellou, L.; Voigt, M.; Giannouli, M.; Kennou, S.; Nelson, J.; Bradley, D. D.; Brabec, C. J. *Adv. Energy Mater.* **2012**, *3*, 391−398.
(19) Huang, J.-H.; Wei, H.-Y.; Huang, K.-C.; Chen, C.-L.; Wang, R.-R.; Chen, F.-C.; Ho, K.-C.; Chu, C.-W. *Energy Environ. Sci.* **2010**, *3*, 654−658.
(20) Park, S. H.; Roy, A.; Beaupré, S.; Cho, S.; Coates, N.; Moon, J. S.; Moses, D.; Leclerc, M.; Lee, K.; Heeger, A. J. *Nat. Photon.* **2009**, *3*, 297−302.
(21) Chen, X.; Mao, S. S. *Chem. Rev.* **2007**, *107*, 2891−2959.
(22) Fujishima, A.; Honda, K. *Nature* **1972**, *238*, 37−38.
(23) O'regan, B.; Grfitzeli, M. *Nature* **1991**, *353*, 737−740.
(24) Chang, W.-F. S.; Chang, C.-P.; Chu, M.-W.; Chen, C.-W. *J. Am. Chem. Soc.* **2009**, *131*, 3644−3649.

(25) Yu, J.; Shen, T. L.; Weng, W. H.; Huang, Y. C.; Huang, C. I.; Su, W. F.; Rwei, S. P.; Ho, K. C.; Wang, L. *Adv. Energy Mater.* **2012**, *2*, 245−252.
(26) Gao, F.; Ren, S.; Wang, J. *Energy Environ. Sci.* **2013**, *6*, 2020−2040.
(27) Lee, K.; Kim, J. Y.; Park, S. H.; Kim, S. H.; Cho, S.; Heeger, A. J. *Adv.Mater.* **2007**, *19*, 2445−2449.
(28) Liao, H.-C.; Lee, C.-H.; Ho, Y.-C.; Jao, M.-H.; Tsai, C.-M.; Chuang, C.-M.; Shyue, J.-J.; Chen, Y.-F.; Su, W.-F. *J. Mater. Chem.* **2012**, *22*, 10589−10596.
(29) Min, C.; Shi, C.; Zhang, W.; Jiu, T.; Chen, J.; Ma, D.; Fang, J. *Angew. Chem., Int. Ed.* **2013**, *52*, 3417−3420.
(30) Cheng, Y.-J.; Cao, F.-Y.; Lin, W.-C.; Chen, C.-H.; Hsieh, C.-H. *Chem. Mater.* **2011**, *23*, 1512−1518.
(31) Hau, S. K.; Yip, H.-L.; Acton, O.; Baek, N. S.; Ma, H.; Jen, A. K.-Y. *J. Mater. Chem.* **2008**, *18*, 5113−5119.
(32) Goh, C.; Scully, S. R.; McGehee, M. D. *J. Appl. Phys.* **2007**, *101*, 114503−114503-12.
(33) Li, S.-S.; Chang, C.-P.; Lin, C.-C.; Lin, Y.-Y.; Chang, C.-H.; Yang, J.-R.; Chu, M.-W.; Chen, C.-W. *J. Am. Chem. Soc.* **2011**, *133*, 11614−11620.
(34) Cozzoli, P. D.; Kornowski, A.; Weller, H. *J. Am. Chem. Soc.* **2003**, *125*, 14539−14548.
(35) Leontie, L.; Druta, I.; Danac, R.; Rusu, G. *Synth. Met.* **2005**, *155*, 138−145.
(36) Kido, J.; Ikeda, W.; Kimura, M.; Nagai, K. *Jpn. J. Appl. Phys.* **1996**, *35*, L394−L396.
(37) Sammes, P. G.; Yahioglu, G. *Chem. Soc. Rev.* **1994**, *23*, 327−334.
(38) Chan, M.-S.; Wahl, A. C. *J. Chem. Phys.* **1978**, *82*, 2542−2549.
(39) Yip, H.-L.; Jen, A. K.-Y. *Energy Environ. Sci.* **2012**, *5*, 5994−6011.
(40) Nishigaki, S.; Yoshioka, H.; Nakatsu, K. *Acta Crystallogr., Sect. B* **1978**, *34*, 875−879.
(41) Robson, F.; de, F.; Airoldi, C. *J. Phys. Chem. Solids* **2003**, *64*, 2199−2204.
(42) Tu, Y.-C.; Lin, J.-F.; Lin, W.-C.; Liu, C.-P.; Shyue, J.-J.; Su, W.-F. *CrystEngComm* **2012**, *14*, 4772−4776.
(43) Lin, J.-F.; Tu, G.-Y.; Ho, C.-C.; Chang, C.-Y.; Yen, W.-C.; Hsu, S.-H.; Chen, Y.-F.; Su, W.-F. *Appl. Mater. Interfaces* **2013**, *5*, 1009−1016.
(44) Ferragina, C.; Massucci, M. A.; Mattogno, G. *J. Inclusion Phenom.* **1989**, *7*, 529−536.
(45) Shi, S.; Schmerber, G.; Arabski, J.; Beaufrand, J.-B.; Kim, D.; Boukari, S.; Bowen, M.; Kemp, N.; Viart, N.; Rogez, G. *Appl. Phys. Lett.* **2009**, *95*, 043303.
(46) Kuznetsov, M.; Zhuravlev, J. F.; Zhilyaev, V.; Gubanov, V. *J. Electron Spectrosc. Relat. Phenom.* **1992**, *58*, 1−9.
(47) Yoon, S. M.; Lou, S. J.; Loser, S.; Smith, J.; Chen, L. X.; Facchetti, A.; Marks, T. *Nano Lett.* **2012**, *12*, 6315−6321.
(48) Lin, Y.-H.; Yang, P.-C.; Huang, J.-S.; Huang, G.-D.; Wang, I.-J.; Wu, W.-H.; Lin, M.-Y.; Su, W.-F.; Lin, C.-F. *Sol. Energy Mater. Sol. Cells* **2011**, *95*, 2511−2515.
(49) Wang, M.; Moon, S. J.; Zhou, D.; Le Formal, F.; Cevey-Ha, N. L.; Humphry-Baker, R.; Grätzel, C.; Wang, P.; Zakeeruddin, S. M.; Grätzel, M. *Adv. Funct. Mater.* **2010**, *20*, 1821−1826.
(50) Voigt, M. M.; Mackenzie, R. C.; King, S. P.; Yau, C. P.; Atienzar, P.; Dane, J.; Keivanidis, P. E.; Zadrazil, I.; Bradley, D. D.; Nelson, J. *Sol. Energy Mater. Sol. Cells* **2012**, *105*, 77−85.
(51) Park, M. H.; Li, J. H.; Kumar, A.; Li, G.; Yang, Y. *Adv. Funct. Mater.* **2009**, *19*, 1241−1246.